doi.org/10.1002/batt.202100106

Evaluating the Passivation Layer of Freshly Cleaved Silicon Surfaces by Binary Silane-Based Electrolytes

Dan Schneier[+],*[a] Yonatan Horowitz[+],[b] Johannes Kasnatscheew,[c] Mariano Grünebaum,[c] Hans-Dieter Wiemhöfer,[c] Martin Winter,[c] and Emanuel Peled*[a]

The expansion of silicon anodes in lithium-ion batteries during lithiation and the resulting instability of its solid-electrolyte interphase (SEI) has been its Achilles heel for quite some time. Beyond the mechanical damage, this expansion exposes fresh elemental silicon to the electrolyte solution. The electrolyte readily decomposes on the reactive silicon surface. Researchers that test novel electrolytes find it difficult to separate which of the electrolyte components (solvent or anion) decomposes first and diagnose the respective decomposition products. Here, we utilize a straightforward test protocol that reveals which reduces first on bare silicon. We exposed four electrolyte mixtures to elemental silicon in custom made T-cells by breaking thin silicon wafers in solution. We analyze the resulting surface film layers and compare their composition to the electrolyte's performance in symmetrical lithium cells, and Si/Li cells. We found that unstable anions rather than reactive solvents lead to poor electrochemical performance.

1. Introduction

The energy density, power, efficiency, shelf life, and lifetime, of lithium ion batteries have been steadily increasing since Sony's engineers had devised the first commercial lithium ion batteries (LIBs) in the 1991.[1,2] The proven record of LIBs as secondary (i.e., rechargeable) batteries in industries ranging from electronics and communication to vehicular and space ones has led to a natural step in their evolution where LIB are envisioned and designed for either grand scale applications, for example, stationary energy storage[3,4] or for micro applications,[5–7] such as medical devices, and wearable electronics.[8,9] We should remind ourselves that despite their wide use and applications, when LIBs are mechanically or electronically abused their chemistry can lead to catastrophic failures.[10–12] Safety enhancement via simple replacement of the ether and carbonate-based electrolyte components with non-flammable counterparts still remains a challenge. Mainly, because electrolyte candidates must meet several requirements simultaneously, starting with physical properties (working temperature range, ion transport, etc.) to chemical ones (stability, chemical compatibility, etc.).[13,14] One of the major chemical requirements from any electrolyte is to produce an effective coating to protect the anode surface. This coating, termed as solid electrolyte interphase (SEI), is crucial to a safe and efficient performance of any LIB.[15] Silane-based coating layers have been shown to provide a good foundation for SEI on silicon anodes thanks to their strong adhesion to silicon particles and the ability to customize their end-groups which come in contact with the electrolyte.[16,17] Beyond that, aprotic liquid electrolytes based on siloxane (R–Si–O–Si–R)[18,19] or silane (R–Si–O–R)[20,21] solvents are promising candidates to replace carbonate-based electrolytes. They are less flammable while providing adequate properties in terms of ionic conductivity over a broad temperature range, as well as sufficient electrochemical stabilities. Thus, silane or siloxane solvents enable safe high voltage applications. In this study we chose two Si–O based solvents. The first, disiloxane-based 1,3-bis(cyanopropyl) tetramethyldisiloxane, a disiloxane with nitrile end groups (TmdSx–CN, Scheme 1a).[22] The second, a silane (2-cynaoethyl) triethoxysilane (2-CTS, Scheme 1b).[23] However, to successfully compete with commercial electrolytes, the ability to form a comparably effective SEI[24] is essential. Grünebaum et. al.[25] were able to synthesize a very stable lithium salt based on trifluoromethyl substituted pyrazolide anion (LiFAP1,1, Scheme 1c). As a case study they compared between an N-heterocyclic lithium salt, to its modified version where they added a BF_3-group at the nitrogen atom. As expected, the modified anion compared to its unmodified version presented higher thermal and electrochemical stabilities, greater ionic conductivity, higher C-rates, and longer cycling performance.

The use of silicon as an anode material has been studied as an alternative to graphite in the lithium-ion battery because of its much higher capacity.[26] Alas, the expansion and contraction

[a] D. Schneier,[+] Prof. E. Peled
School of Chemistry, Faculty of Exact Sciences
Tel Aviv University
Tel Aviv, 6997801, Israel
E-mail: danschneier@mail.tau.ac.il
peled@tauex.tau.ac.il
[b] Dr. Y. Horowitz[+]
The Faculty of Digital Medical Technologies
Holon Institute of Technology
Holon 5810201, Israel
[c] Dr. J. Kasnatscheew, Dr. M. Grünebaum, Dr. H.-D. Wiemhöfer, Prof. M. Winter
Forschungszentrum Jülich GmbH
Helmholtz-Institute Münster, IEK-12
Corrensstraße 46, 48149 Münster, Germany
[+] These authors contributed equally to this work.

Supporting information for this article is available on the WWW under https://doi.org/10.1002/batt.202100106

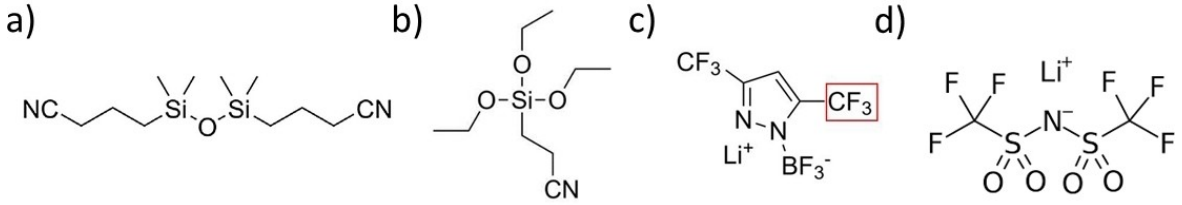

Scheme 1. The two examined solvents a) TmdSx–CN, b) 2-CTS, and the two examined salts c) LiFAP1,1, d) LiTFSI.

of silicon based anodes during the charge/discharge of lithium-ion batteries has been its Achilles heel for quite some time.[27] During lithiation, the silicon lattice expands up to 300% to accommodate the lithium ions.[28] This expansion in silicon may lead to mechanical pulverization of the silicon itself and is the primary cause of the repetitive electrolyte reduction on the dynamic SEI layer.[24] Computational studies have also shown that the expansion of silicon may also lead to lower porosity and decreased diffusion coefficient of lithium in the anode, even when silicon is mixed with large amounts of graphite.[29,30] While the majority of the SEI is formed in parallel with the first lithiation, silicon expansion during initial cycles, like other Li storage metals,[31] exposes fresh elemental silicon to the electrolyte solution. The electrolyte, which is composed of at least one organic, aprotic solvent and a lithium salt[13] readily decomposes on the highly reactive fresh silicon surface[28] to form a protective layer that slows further reduction. This initial protection serves as the basis of the SEI which evolves with cycling, and therefore affects its structure and composition. In previous works, we have presented a simple and effective method to expose elemental silicon to battery electrolytes in a Li metal based cell configuration (silicon versus lithium) by cleaving silicon wafers inside the cell, and we demonstrated how a common electrolyte additive, fluoroethylene carbonate, affects the SEI formation on the exposed silicon.[32,33] Here we further expand on this method by testing four different electrolyte compositions, made with two different salts- the abovementioned LiFAP1,1 and the commonly used lithium bis (trifluoromethanesulfonyl) imide (LiTFSI, Scheme 1d)[34,35] and 2 silane-based solvents. We analyze silicon surfaces passivated by these electrolytes, and compare their electrochemical features with the ones deduced from cycling performance of Li/Li symmetric cells and the capacity retention of Si/Li cells.

2. Results and Discussion

The four electrolytes tested in this work are different combinations of the two salts and two solvents presented in Scheme 1. The electrolytes were mixed in the glovebox with a magnetic stirrer, and all but the mixture of LiFAP1,1 in TmdSx–CN were fully dissolved within hours. The LiFAP1,1 in TmdSx–CN electrolyte remained murky even after continuous stirring, suggesting poor solubility of the salt in that solvent.

2.1. Electrochemical Analysis, OCV Profiles

All immersed silicon wafers reached an equilibrium within 30 minutes reflected by a stable open circuit voltage (OCV). Upon the wafers break, i.e., exposing the electrolyte to fresh elemental silicon we detected a drop in the OCV profiles (Figure 1). Generally, the two electrolytes with the 1 M LiTFSI salt, in TmdSx–CN (denoted as electrolyte #1) and in 2-CTS (denoted as electrolyte #2) showed a different behavior than those with 1 M LiFAP1,1 (denoted as #3 for TmdSx–CN, and #4 for 2-CTS), with subtler differences between electrolytes #1 and #2. Both electrolytes with the $TFSI^-$ anion (#1 and #2) exhibit two consecutive drops in their OCV profiles upon exposure to elemental silicon. The first and sharp drop is reached within 3–5 ms. The Si/Li cell with electrolyte #1 dropped by ~290 mV, while the cell with #2 dropped by ~360 mV. The second minimum of the two electrolytes is dependent on the solvent. Electrolyte #1 (1 M LiTFSI salt, in TmdSx–CN) reached its second minimum after ~4 seconds, and did not recover to its initial OCV. However, electrolyte #2 (same anion but in 2-CTS) reached its second minimum within ~50 ms, and recovered to ~90% of its initial OCV within 20 seconds. We have concluded in our previous studies that the rapid stabilization of the OCV after the wafers break indicates a quick and effective protection of the surface.[32,33] We suggest that the two consecutive minima indicate that the protection of the surface can be separated to the specific decomposition of the lithium salt, and solvent. The OCV does not return to its original value for two reasons. The first is that while the passivation of the surface is incomplete redox reactions continue to take place and cause a shift in the voltage of the cell. The second reason is that the new surface layer on the silicon has in itself a different chemical potential than the native oxide and therefore the OCV will be permanently shifted, as exemplified in our previous study with carbonate-based electrolytes.[32]

For electrolytes #3 and #4 that contain LiFAP1,1 salt, the behavior of the OCV after the break is harder to characterize. For both electrolytes the OCV constantly fluctuated before and after the break (Figure 1c–d, red curves). We assume that a continuous decomposition process occurred on the electrodes surface in these electrolytes. Therefore, to ease our analysis we smoothed the OCV data (100 points average, black curves in Figure 1c–d). Electrolyte #3 (1 M LiFAP1,1 in TmdSx–CN), which was the only electrolyte not to show complete optical dissolution of the salt, showed a voltage drop during cleaving of only ~30 mV. In addition, when we disassembled the cell,

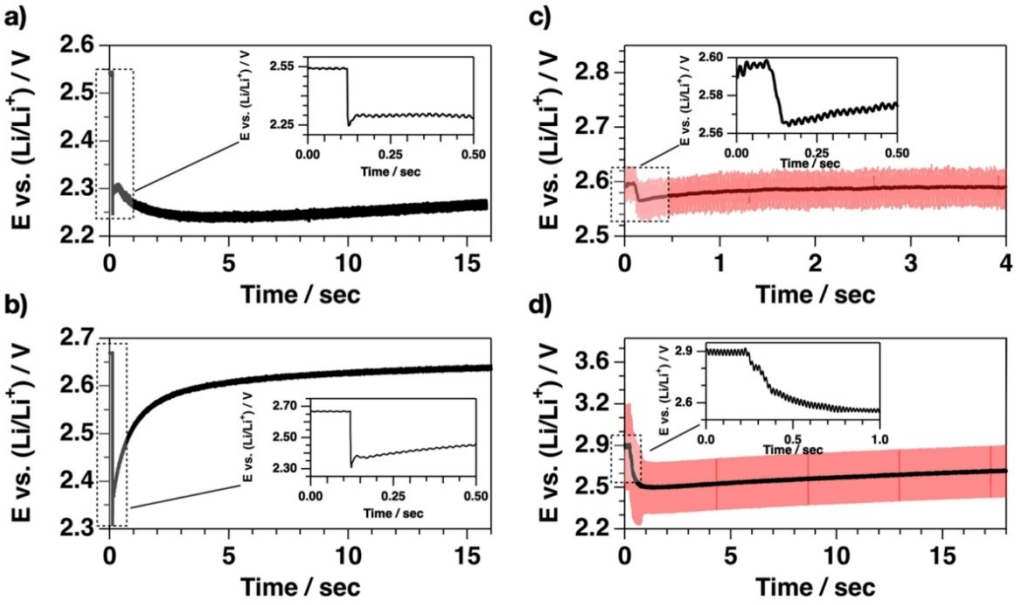

Figure 1. Voltage profiles of the Si/Li cells upon cleavage in: a) 1 M LiTFSI in TmdSx–CN, b) 1 M LiTFSI in 2-CTS, c) 1 M LiFAP1,1 in TmdSx–CN, and d) 1 M LiFAP1,1 in 2-CTS.

we found that the lithium electrode was covered by a visible white film. Therefore, we suggest that in addition to the decomposition reactions of the electrolyte on the Si surface, some adsorption reactions or precipitation of the salt add to the surface film formation process. The partial dissolution may also mean a lower effective concentration of the solution, which in turn could also lead to the small voltage drop after the break. The OCV profile of electrolyte #4 (1 M LiFAP1,1 in 2-CTS) had the largest fluctuations in OCV, roughly 0.3 V in amplitude. When smoothed, the OCV plot shows a ~0.3 V drop upon cleavage, similar to samples #1 and #2, and the average OCV regained 40% of its initial value after 20 seconds. We suggest that the erratic behavior of sample #4 is the result of ongoing decomposition on the surface that forms a protective layer that dissolves and reforms constantly even at OCV. The OCV changes of the 4 electrolytes are summarized in in the Supporting Information Table 1.

2.2. Surface Film Layer Imaging by SEM

To image the resulting surface film layers after cleaving by SEM, we rinsed the Si wafer fragments with THF to remove residual electrolyte solution and immediately dried them under vacuum. We present the SEM images of the four samples in Figure 2. In samples #1 and #2, with the LiTFSI salt, there are no noticeable surface film products on the surface, implying that the surface passivation layer is too thin to be detected by SEM. Sample #3, on the other hand, displays a thick, web-like surface layer with scattered lumps covered with tendrils that stretch across the Si surface. Sample #4 shows scattered particles attached to the surface, but without the web-like features of #3.

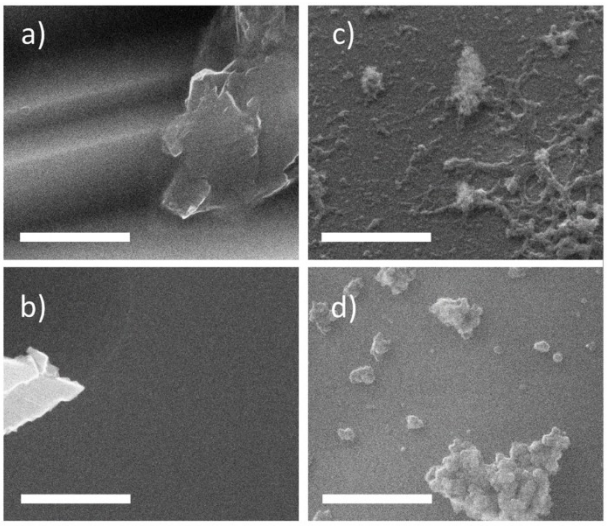

Figure 2. SEM images of the cleaved Si wafers surface. a) in 1 M LiTFSI in TmdSx–CN, b) in 1 M LiTFSI in 2-CTS, c) in 1 M LiFAP1,1 in TmdSx–CN, d) in 1 M LiFAP1,1 in 2-CTS. The scale bar equals 1 μm.

2.3. Depth Profile and High-Resolution XPS

We have carried out ex situ high-resolution XPS (HR-XPS) and depth profile XPS (DP-XPS) measurements to determine the chemical composition on the exposed silicon surface after the electrolytes' spontaneous decomposition.[36–39] In Figure 3, we present the atomic concentrations as a function of sputter time (DP-XPS) of the four electrolytes. Compared to the three others, electrolyte #3 has the thickest layer which matches the visible surface shown in Figure 2 and might help explain the stability of the voltage in Figure 1.

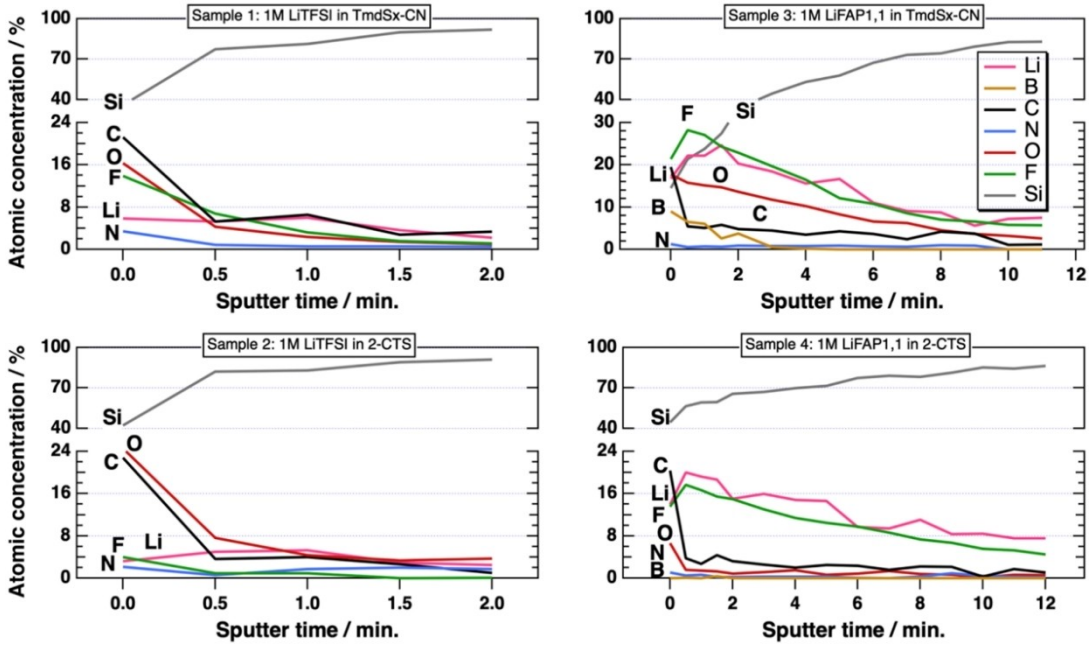

Figure 3. The depth-profile XPS of the surface coating following spontaneous decomposition at the bare silicon surface of the four electrolytes: 1) 1 M LiTFSI in TmdSx–CN, 2) 1 M LiTFSI in 2-CTS, 3) 1 M LiFAP1,1 in TmdSx–CN, and 4) 1 M LiFAP1,1 in 2-CTS.

We chose the two salts since both have CF_3 groups (LiFAP1,1 also has a unique –N–BF_3 group) that have binding energy peaks in the C 1s spectrum at 293–294 eV[38] making them distinguishable from the CN groups of the solvents. In the following section we present each sample's C 1s, N 1s, and Si 2p HR-XPS spectra that were obtained from three layers of the spontaneous decomposition thin film. The first layer is the electrolyte-thin film interphase (0 minutes sputter), the second, the bulk decomposition layer (0.5 minutes sputter), and finally close to the Si (2 minutes of sputter).

In Figure 4, we present the HR-XPS spectra of sample #1 (1 M LiTFSI dissolved in TmdSx–CN). When we examine the chemical composition found on the Si surface (2 minutes of sputter) we propose that Si–C is present with typical binding

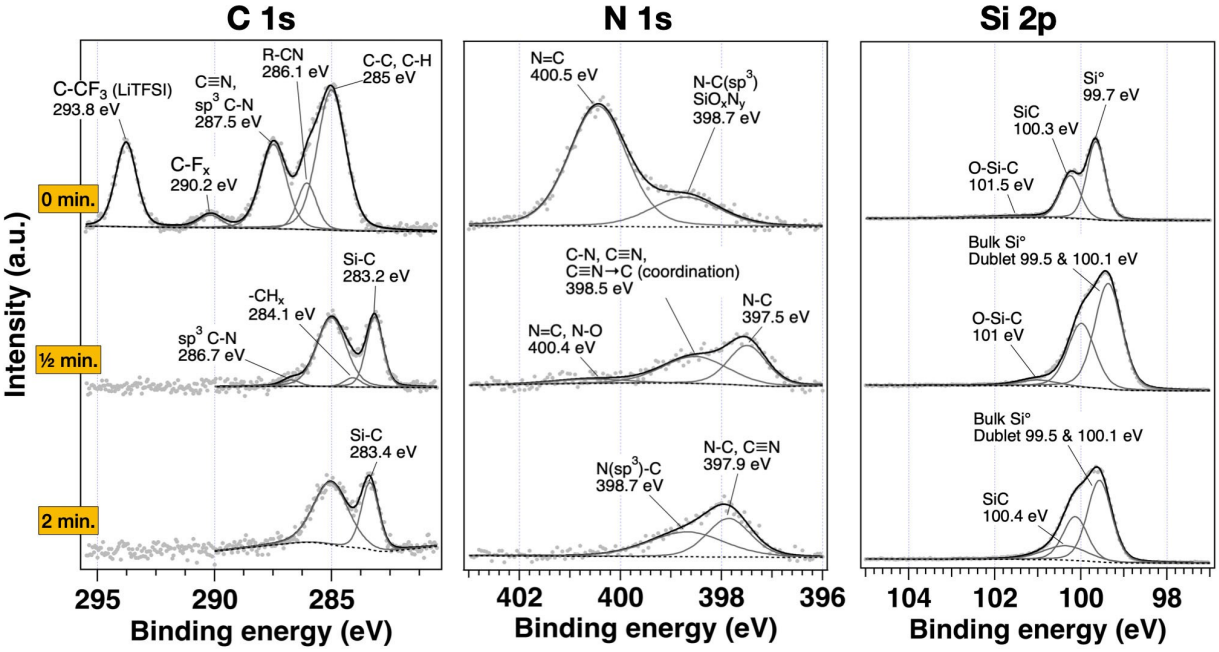

Figure 4. HR-XPS spectra of 1 M LiTFSI dissolved in TmdSx–CN (sample #1). To emphasize the relative abundance of the species at various depths (0, $^1/_2$, and 2 minutes of sputtering) we have maintained the spectra intensities but shifted them vertically.

energy peaks at C 1s 283.4 eV, and Si 2p 100.4 eV) together with C–N species (N 1s 397.9 eV CN, C–N and N(sp^3)–C at 398.7 eV). We note that there are no binding energy peaks assigned to LiTFSI. We therefore suggest that either there is a residual dissociation of the $TFSI^-$ anion or that the TmdSx–CN dissolved first.

Our suggestion is further corroborated by the composition of the bulk thin layer (0.5 minutes sputter). Here, both the C 1s and N 1s spectra only show binding energy peaks relevant to the dissociation of the solvent to its constituents of C, N and O–Si–C bonds. For example, C–N (C 1s 286.7 eV, N 1s 397.5 eV), CN and C–N at 398.5 eV, and C=N at N 1s 400.4 eV. Still, we find no noticeable presence of the anion salt.

Only at the electrolyte-thin film interface, we clearly detect the $TFSI^-$ anion by its characteristic binding energy peaks of C 1s 293.8 eV (and S 2p 170 eV, O 1s 533.8 eV found in the Supporting Information Figure S2. We also observe CN (C 1s 287.5 eV), C=N (N 1s 400.5 eV), and C–N sp^3 (C 1s 287.5 eV, N 1s 398.7 eV) groups. In addition to the CN binding energy peaks, we detect O–Si–C at Si 2p 101.5 eV. All these groups (binding energies) can only originate from the TmdSx–CN solvent. Thus, we conclude that the disiloxane solvent appears to partially react with the elemental Si surface.

In Figure 5, we present the HR-XPS spectra of sample #2 (1 M LiTFSI solvated in 2-CTS). Right on the surface of the Si (2 min. sputter) we observe Si–C species (C 1s 283.2 eV). In the N1s spectrum we see binding energy peaks see at 399 eV, and 397.9 eV that we assign to CN, Si_xN_y or C–N species, respectively. At the bulk of the coating film (0.5 minute sputter) we observe various species that we presume to originate from the silane solvent. For example, in the N1s spectrum we observe Si_xN_y (or C–N) species and C≡N and C–N species that are associated with 2-CTS. While in the C 1s spectrum we notice that only Si–C at 283.1 eV and the C–C at 285 eV are present. As in the case of sample #1, we do not find a noticeable presence of the anion $TFSI^-$ after minimal sputtering. Similar to sample #1, we do find characteristic binding energy peaks of LiTFSI in the layer in contact with the electrolyte (i.e., 0 min. sputter). Here, we spot the same species as in sample #1 only with minor (~0.4 eV) BE shifts. We further notice the presence of SiO_2 (Si 2p 102.8 eV) that could have resulted from the dissociation of the C–O–Si bonds found in the 2-CTS solvent. Therefore, we suggest that the disiloxane solvent reacts with the Si surface before the $TFSI^-$ anion does.

In Figure 6, we present the HR-XPS spectra of sample #3 (1 M LiFAP1,1 solvated in TmdSx–CN). From a bird's view, it seems that the FAP1,1 anion partially reacts with the bare Si surface. We can monitor the anion presence by the N–BF_3 groups at B 1s ~194.8 eV and possible (Li)BF_4 groups at 195.9 eV (Supporting Information Figure S3). At the electrolyte-thin film interphase (0 min. sputter), we monitor the anion presence by C, N bonds emanating from the ring opening as C–N (e.g., C 1s 286.5 eV, N 1s 398.5 eV) as well as other organometallic with N species at N 1s ~404.3 eV. Indeed, at the Si surface (2 min. sputter) we notice the presence of the *N*-hetero ring constitutes in the N 1s spectrum where the C–N peak (397.8 eV) is almost as strong as the C≡N peak (~400 eV) that we associate to the solvent's cyanic group. And, in the B 1s spectrum we point to the prominent peak of the N–BF_3 group at 195.5 eV, and to B–oxide (193.2 eV, supporting info Figure S3).

Looking at the bulk layer spectra after 0.5 minutes of sputtering we see bonds of O–Si–C (C 1s 283.3 eV), CN groups (N 1s 400.5 eV) but no Si–C or Si–O species, originating from the solvent. Furthermore, we detect the reaction products of the LiFAP1,1 N-heterocyclic ring with the elemental silicon by

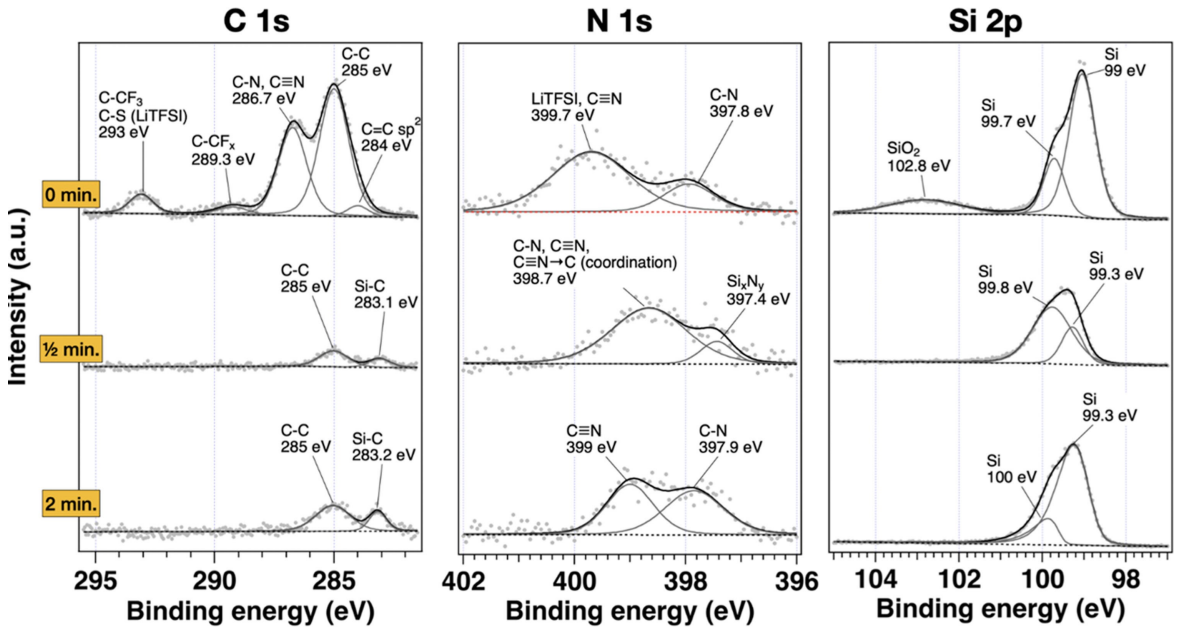

Figure 5. HR-XPS spectra of 1 M LiTFSI solvated in 2-CTS (sample #2). To emphasize the relative abundance of the species at various depths (0, ½, and 2 minutes of sputtering) we have maintained the spectra intensities but shifted them vertically.

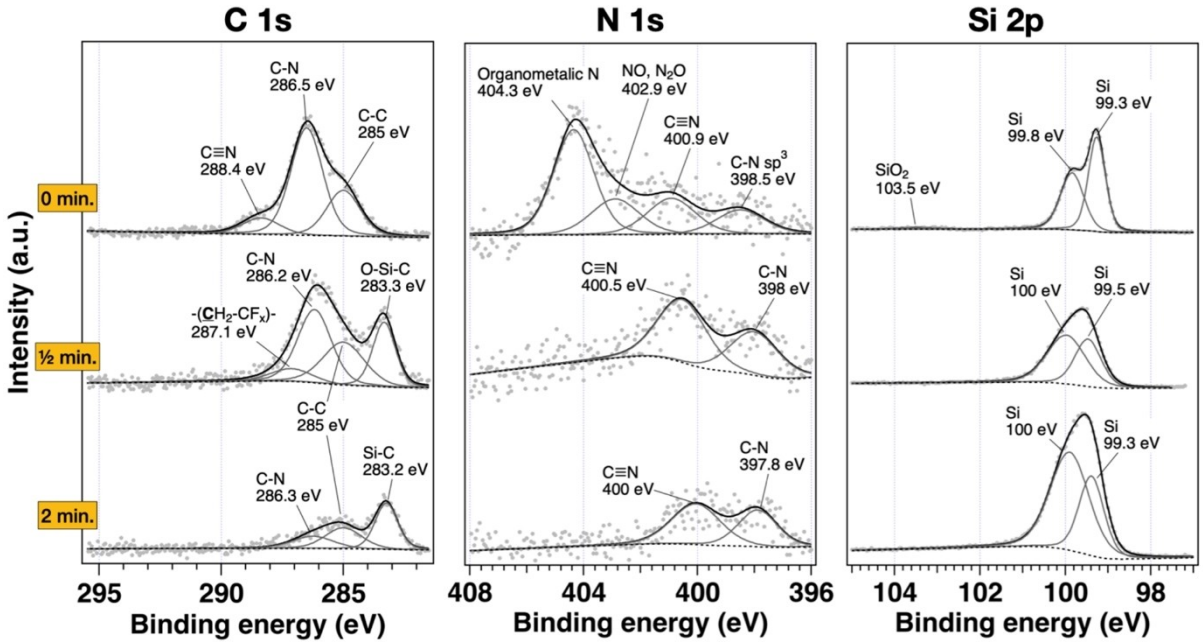

Figure 6. HR-XPS spectra of 1 M LiFAP1,1 solvated in TmdSx–CN (sample #3). To emphasize the relative abundance of the species at various depths (0, $^1/_2$, and 2 minutes of sputtering) we have maintained the spectra intensities but shifted them vertically.

energy binding peaks that we assign to –(CH_2–CF_x)– moieties (C 1s 287.1 eV), the N–BF_3 group (B 1s 195.5 eV), and C–N species (C 1s 286.2 eV, N 1s 398 eV). The binding energy of the N–BF_3 group is slightly shifted. We presume that this shift is due to the group proximity to the Si surface. We also detect possible B–oxides (B 1s 193.4 eV).

Overall, sample #3 coating layer is thicker than the other samples since the sputter continues for 12 minutes. At the upper section of this layer (0 minutes sputter) we detect the $FAP1,1^-$ anion by the N–BF_3 group at B 1s 194.8 eV and possible (Li)BF_4 groups at 195.9 eV. We also note various carbon–nitrogen bonds from the ring opening as C–N (C 1s 286.5 eV, N 1s 398.5 eV) as well as other organometallic with N species at N 1s 404.3 eV. Despite having the highest F content (22 %at), we see no CF_3 groups. In fact, the analysis of the DP-XPS profiles suggest that most of the fluorine is present in the form of LiF and BF_3.

It is our understanding, that the presence of both salt and solvent decomposition entities before and after 2 minutes of sputtering suggests that the salt and solvent decompose simultaneously, perhaps even trapping some deposited species inside the decomposition layer as we reported in a previous paper.[22]

In Figure 7, we present the HR-XPS spectra of 1 M LiFAP1,1 solvated in 2-CTS (sample #4).

The Si 2p spectra of the wafers' surface, and bulk layer of sample #4 are dominated by elemental silicon peaks (Si 2p ~99.5 eV and ~99.0 eV). The C1s spectra are limited to C–N (287.1 eV) bonds and Si–C (283 eV) ones. Only at the decomposition layer interface with the electrolyte do we detect binding energy peaks associated with the N-heterocyclic anion. For example, at N 1s we notice the N–BF_3 at 402.1 eV together with CN (399.9 eV) and C–N (397.9 eV) species that we assume belong to the 2-CTS solvent. In the C1s spectrum we detect the anion's C-CF_x goups at 289.3 eV (CN), and C–N solvent groups at 286.8 eV (C–N). In this sample, we find a weak presence of the salt on the surface. The fact that it has the second thickest decomposition layer suggests that solvent (2-CTS) reacts with the bare silicon well before the anion does. These findings not only shed light on the specific electrolyte solutions we display in this manuscript, but also further exemplify that our method of cleaving Si wafers inside the cells can be used for fast and fundamental evaluation of electrolyte stability on reactive surfaces.

2.4. EIS Measurements of Li/Li Cells

Cycling electrolytes in Li/Li symmetric cells is a common practice aimed to evaluate the stability of new electrolytes vs. Li metal anodes. It parallels silicon cleaving in that it exposes a highly reactive electrode surface to the electrolyte. Therefore, we wanted to test if our four electrolytes present the same stability results (obtained from the silicon cleaving protocol) in Li/Li symmetric cells, meaning our method would be transferable between different electrodes. We began with EIS measurements taken at rest with increasing time intervals from 1 h to a full week (168 h). After a week at rest conditions, we cycled the same symmetrical Li/Li cells to assess the evolution of the overpotential on the lithium electrodes. The EIS spectra (at rest) of the cells at increasing times are presented in Figure 8a–d. The equivalent circuit used for fitting values to the spectra is presented in Figure 8b. The intercept with the X-axis at high frequencies represents the ionic resistance of the

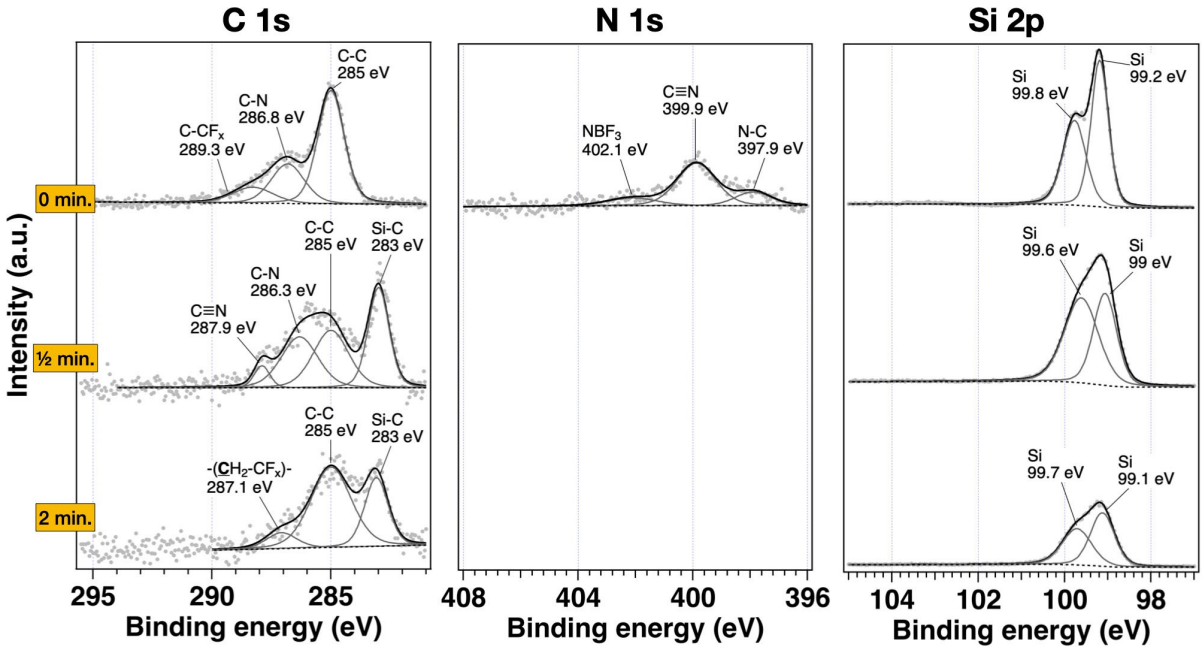

Figure 7. HR-XPS spectra of 1 M LiFAP1,1 solvated in 2-CTS (sample #4). To emphasize the relative abundance of the species at various depths (0, $^{1}/_{2}$, and 2 minutes of sputtering) we have maintained the spectra intensities but shifted them vertically.

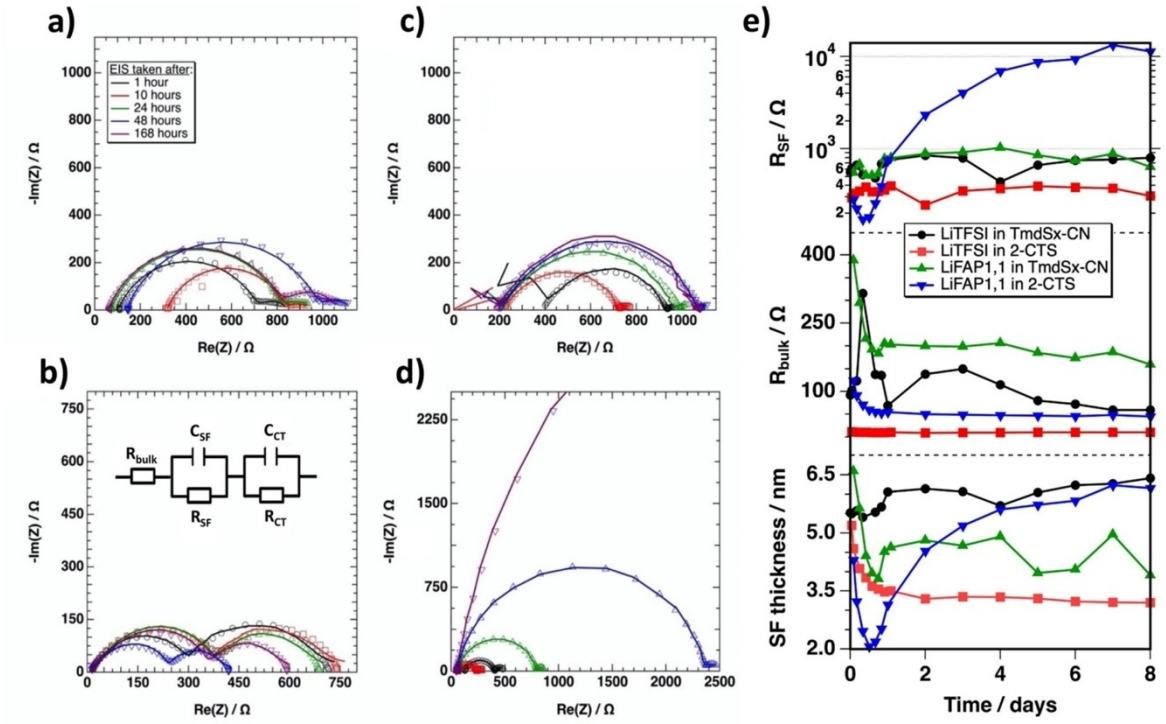

Figure 8. EIS of Li/Li symmetric cells at rest over one week in: a) 1 M LiTFSI in TmdSx–CN, b) 1 M LiTFSI in 2-CTS, c) 1 M LiFAP1,1 in TmdSx–CN, d) 1 M LiFAP1,1 in 2-CTS, and e) summary of fitting parameters for the surface film layer (SF). We illustrate the equivalent circuit used for fitting the EIS data at b.

electrolyte (R_{bulk}) and the two semicircles represent the resistance and capacitance of the surface film (SF) and of charge transfer (CT) on the electrodes, respectively.[40] The thickness of the surface film layer (d_{SF}) was calculated by extracting the capacitance (C_{SF}) of the passivating layer and using Equation (1).[41]

$$d_{SF} = \frac{\varepsilon \varepsilon_0 A}{C_{SF}} \quad (1)$$

Where ε is the dielectric constant of the passivation layer (= 10),[15] and A is the surface area of the lithium electrodes (2× 15 mm wide discs). The evolution in time of R_{bulk}, R_{SF} and d_{SF} is shown in Figure 8e. The silane (2-CTS) solvent resulted in lower R_{bulk} than the siloxane (TmdSx–CN), most likely since the LiFAP1,1 salt did not dissolve properly. The R_{SF} and d_{SF} of electrolyte #4 (1 M LiFAP1,1 in 2-CTS) change the most over time. Over the first 12 h their bulk resistance decreases followed by a monotonous increase reaching an R_{SF} value that is an order of magnitude higher than all the other cells. It seems that the initial R_{SF} values are specific to the solvent regardless of the lithium salt. This R_{SF} correlation goes hand in hand with our XPS and OCV data analysis on which we suggest that the solvents are first to react with the silicon fresh surface rather than the anions.

In short, we suggest that the primary passivation layer on the elemental silicon comprises of insoluble reaction products of silane and disiloxane. In samples #1 and #2, both containing LiTFSI, we see lower R_{bulk}, R_{SF}, and d_{SF} values signifying better passivation when the LiTFSI salt is dissolved in the 2-CTS solvent (sample #2). Again, we reached the same conclusion based on our voltage profile analysis of the cleaved Si/Li cells.

After their period of rest, we cycled all the symmetric cells at 0.1 mA for 1 h (40 cycles). We present the resulting overpotential of the different cells in the Supporting Information Figure S4. Once again, sample #4 shows the largest overpotential by an order of magnitude, and the lowest overpotential belongs to sample #2.

Finally, we wished to test these new electrolytes in contact with actual Si-based electrodes and so we assembled cells with Si/Ni/C composite electrodes versus lithium.[42] The specific capacities vs. cycles of the cells are shown in Figure 9. In early studies we found that when using silane electrolytes even small amounts of carbonate-based additives are crucial for the formation of an effective SEI on silicon based anodes.[22] However, to directly compare the silane or siloxane electrolyte performances to the ones we report in this paper (i.e., without any additives) we cycled three electrolytes (samples #1, #2, and #4) without any additives. We discarded electrolyte #3 due to its initial problematic solubility and high R_{bulk} (~10^4 Ω). The cells were cycled at 50 μA for 10 cycles. As we expected the specific capacity of the cells without additives is low. Cells with electrolytes #1 (1 M LiTFSI in TmdSx–CN), and #2 (1 M LiTFSI in 2-CTS) show low capacities. For sample #2, we notice a high delithiation capacity insinuating that sample #2 suffers from parasitic side reactions that distort the delithiation process. Sample #4 (LiFAP1,1 in 2-CTS), which showed in all previous tests the most unstable surface passivation, yields the highest initial capacity out of all electrolytes. However, the capacity of sample #2 is the only one that increases, while those of sample #1, and #4 degrade rapidly.

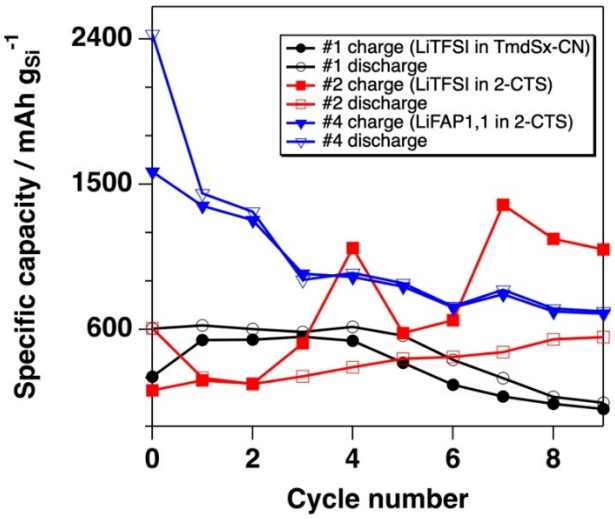

Figure 9. Specific capacity of Si/Li cells over 10 cycles of the different electrolytes: 1) 1 M LiTFSI in TmdSx–CN, 2) 1 M LiTFSI in 2-CTS, and 4) 1 M LiFAP1,1 in 2-CTS.

Based on our cycling analysis, we deduce that the electrolytes with LiTFSI dissolved in either a disiloxane (TmdSx–CN, electrolyte #1) or silane (2-CTS, electrolyte #2) form a highly stable but lithium cation non-permeable (thus non-SEI-type) film on the silicon anodes. Whereas, LiFAP1,1 dissolved in 2-CTS (electrolyte #4) forms an unstable Si passivating layer that turn over into a highly permeable SEI, allowing for several cycles with high capacity before fading. Our conclusions, based on both electrochemical (Figure 1), and layer composition (Figure 3) support this assertion, as the passivation of samples #1, and #2 is rapid but almost devoid of lithium while sample #4 shows a much thicker and a lithium rich interphase.

3. Conclusions

We studied the spontaneous decomposition of binary, silane-based electrolytes in contact with freshly exposed elemental silicon. We found a correlation between the OCV drop in Si/Li cells to the composition of the protection layer spontaneously formed on the silicon surface. We were able to separate the anion decomposition from the solvent one. We conclude that the anion stability rather than the solvent stability is critical to form an effective ion-conductive surface film layer. We corroborate our conclusion by surface analysis methods such as XPS, and SEM, as well with EIS results. Finally, we advocate the addition of our straight-forward protocol to the toolbox of electrolyte developers to assess the protective properties of new electrolytes on reactive surfaces.

Experimental Section

The full details of the methods and procedures used here are provided in the Supporting Information.

Acknowledgements

This work was graciously funded by the German/Israeli Battery School (GIBS) program, grant No. 00040024000. Also, financial support from the German Federal Ministry for Education and Research within the project Galilee (grant number: 13XP0137) is gratefully acknowledged. The authors would like to express their gratitude for Dr. Larisa Burstein and Dr. Pini Shekhter help with the XPS measurements.

Conflict of Interest

The authors declare no conflict of interest.

Keywords: batteries · electrolytes · passivation layers · reaction mechanisms · silicon

[1] Y. Nishi, *J. Power Sources* **2001**, *100*, 101–106.
[2] M. Winter, B. Barnett, K. Xu, *Chem. Rev.* **2018**, *118*, 11433.
[3] B. Dunn, H. Kamath, J. Tarascon, *Science* **2011**, *334*, 928–936.
[4] N. Kittner, F. Lill, D. M. Kammen, *Nat. Energy* **2017**, *2*, 1–6.
[5] D. Golodnitsky, M. Nathan, V. Yufit, E. Strauss, K. Freedman, L. Burstein, *Solid State Ionics* **2006**, *177*, 2811–2819.
[6] M. Roberts, P. Johns, J. Owen, D. Brandell, K. Edstrom, E. Enany, C. Guery, D. Golodnitsky, M. Lacey, C. Lecoeur, H. Mazor, E. Peled, E. Perre, M. M. Shaijumon, P. Taberna, *J. Mater. Chem.* **2011**, *21*, 9876–9890.
[7] R. Schmuch, R. Wagner, G. Hörpel, T. Placke, M. Winter, *Nat. Energy* **2018**, *3*, 267–278.
[8] D. G. Mackanic, X. Yan, Q. Zhang, N. Matsuhisa, Z. Yu, Y. Jiang, T. Manika, J. Lopez, H. Yan, K. Liu, X. Chen, Y. Cui, Z. Bao, *Nat. Commun.* **2019**, *10*, 1–11.
[9] R. Kumar, J. Shin, L. Yin, J. You, Y. S. Meng, J. Wang, *Adv. Energy Mater.* **2017**, *7*, 1602096.
[10] D. P. Finegan, E. Darcy, M. Keyser, B. Tjaden, T. M. M. Heenan, R. Jervis, J. J. Bailey, N. T. Vo, O. V. Magdysyuk, M. Drakopoulos, M. Di Michiel, A. Rack, G. Hinds, D. J. L. Brett, P. R. Shearing, *Adv. Sci.* **2018**, *5*, 1700369.
[11] X. Feng, M. Ouyang, X. Liu, L. Lu, Y. Xia, X. He, *Energy Storage Mater.* **2018**, *10*, 246–267.
[12] B. Ng, P. T. Coman, E. Faegh, X. Peng, S. G. Karakalos, X. Jin, W. E. Mustain, R. E. White, *ACS Appl. Mater. Interfaces* **2020**, *3*, 3653–3664.
[13] V. Etacheri, R. Marom, R. Elazari, G. Salitra, D. Aurbach, E. Environ, V. Etacheri, R. Marom, R. Elazari, G. Salitra, D. Aurbach, *Energy Environ. Sci.* **2011**, *4*, 3243–3262.
[14] J. F. Rohan, M. Hasan, S. Patil, D. P. Casey, T. Clancy, in *Energy Storage Batter. Mater. Archit. Nanoscale*, **2014**, pp. 63–94.
[15] E. Peled, *J. Electrochem. Soc.* **1979**, *126*, 2047.
[16] S. Jiang, B. Hu, R. Sahore, L. Zhang, H. Liu, L. Zhang, W. Lu, B. Zhao, Z. Zhang, *ACS Appl. Mater. Interfaces* **2018**, *10*, 44924–44931.
[17] W. Liu, H. Li, J. Jin, Y. Wang, Z. Zhang, Z. Chen, Q. Wang, Y. Chen, E. Paek, D. Mitlin, *Angew. Chem. Int. Ed.* **2019**, *58*, 16590–16600; *Angew. Chem.* **2019**, *131*, 16743–16753.
[18] B. Pohl, M. M. Hiller, S. M. Seidel, M. Grünebaum, *J. Power Sources* **2015**, *274*, 629–635.
[19] B. Pohl, M. Grünebaum, M. Drews, S. Passerini, M. Winter, H. Wiemhöfer, *Electrochim. Acta* **2015**, *180*, 795–800.
[20] K. Amine, Q. Wang, D. R. Vissers, Z. Zhang, N. A. A. Rossi, R. West, *Electrochem. Commun.* **2006**, *8*, 429–433.
[21] Y. Kusachi, J. Dong, Z. Zhang, K. Amine, *J. Power Sources* **2011**, *196*, 8301–8306.
[22] Y. Horowitz, I. Ben-Barak, D. Schneier, M. Goor-Dar, J. Kasnatscheew, P. Meister, M. Grünebaum, H.-D. Wiemhöfer, M. Winter, D. Golodnitsky, E. Peled, *Batteries & Supercaps* **2019**, *2*, 213–222; Supercaps **2019**, 2, 213–222.
[23] F. Aupperle, N. Von Aspern, D. Berghus, F. Weber, G. G. Eshetu, M. Winter, E. Figgemeier, *ACS Appl. Mater. Interfaces* **2019**, *2*, 6513–6527.
[24] E. Peled, S. Menkin, *J. Electrochem. Soc.* **2017**, *164*, A1703–A1719.
[25] M. Grünebaum, A. Buchheit, D. Krause, M. M. Hiller, C. Schmidt, M. Winter, H. Wiemhöfer, *Electrochim. Acta* **2018**, *286*, 313–323.
[26] V. Aravindan, Y. Lee, S. Madhavi, *Adv. Energy Mater.* **2015**, *5*, 1402225.
[27] D. Larcher, S. Beattie, M. Morcrette, K. Edstro, J.-C. Jumas, J. Tarascon, *J. Mater. Chem.* **2007**, *17*, 3759–3772.
[28] L. Y. Beaulieu, K. W. Eberman, R. L. Turner, L. J. Krause, J. R. Dahn, *Electrochem. Solid-State Lett.* **2001**, *4*, A137–A140.
[29] S. Dhillon, G. Hernández, N. P. Wagner, A. M. Svensson, D. Brandell, *Electrochim. Acta* **2021**, *377*, 138067.
[30] R. Chandrasekaran, T. F. Fuller, *J. Electrochem. Soc.* **2011**, *158*, A859–A871.
[31] M. Wachtler, J. O. Besenhard, M. Winter, *J. Power Sources* **2001**, *94*, 189–193.
[32] E. Peled, D. Schneier, Y. Shaham, G. Ardel, L. Burstein, Y. Kamir, *J. Electrochem. Soc.* **2019**, *166*, 2091–2095.
[33] D. Schneier, Y. Shaham, G. Ardel, L. Burstein, Y. Kamir, E. Peled, *J. Electrochem. Soc.* **2019**, *166*, 4020–4024.
[34] M. Marinaro, M. Weinberger, M. Wohlfahrt-Mehrens, *Electrochim. Acta* **2016**, *206*, 99–107.
[35] C. Weller, H. Althues, S. Kaskel, M. Piwko, *J. Power Sources* **2017**, *362*, 349–357.
[36] C. Xu, F. Lindgren, B. Philippe, M. Gorgoi, F. Bjorefors, K. Edstrom, T. Gustafsson, *Chem. Mater.* **2015**, *27*, 2591–2599.
[37] M. Nie, D. P. Abraham, Y. Chen, A. Bose, B. L. Lucht, *J. Phys. Chem. C* **2013**, *117*, 13403–13412.
[38] F. Lindgren, C. Xu, L. Niedzicki, M. Marcinek, T. Gustafsson, F. Bjorefors, K. Edström, R. Younesi, *ACS Appl. Mater. Interfaces* **2016**, *8*, 15758–15766.
[39] G. G. Eshetu, T. Diemant, S. Grugeon, R. J. Behm, S. Laruelle, M. Armand, S. Passerini, *ACS Appl. Mater. Interfaces* **2016**, *8*, 16087–16100.
[40] G. Bieker, M. Winter, P. Bieker, *Phys. Chem. Chem. Phys.* **2015**, *17*, 8670–8679.
[41] R. R. Gaddam, L. Katzenmeier, X. Lamprecht, A. S. Bandarenka, *Phys. Chem. Chem. Phys.* **2021**, 23, 12926-12944.
[42] D. Schneier, Y. Shaham, K. Goldshtein, M. Goor, D. Golodnitsky, E. Peled, *J. Electrochem. Soc.* **2019**, *166*, 740–746.

Manuscript received: May 12, 2021
Revised manuscript received: June 16, 2021
Accepted manuscript online: June 23, 2021
Version of record online: July 5, 2021

Correction added on 07. July 2021, after first online publication: a correction was made to Figure 5.